SSRG International Journal of Electrical and Electronics Engineering
ISSN: 2348-8379/ https://doi.org/10.14445/23488379/IJEEE-V9I12P107

Volume 9 Issue 12, 81-100, December 2022

Original Article

Three-Phase Cascaded Nine-Level Inverter for Grid-Connected Solar PV System

Ch. Santosh Kumar[1], S. Tara Kalyani[2]

[1]*Department of EEE, BVRITH, Hyderabad, India*
[2]*Department of EEE, JNTUH, Hyderabad, India.*

[1]*Corresponding Author : chksantosh@yahoo.com*

Received: 16 October 2022 Revised: 23 November 2022 Accepted: 08 December 2022 Published: 25 December 2022

Abstract *- A hybrid approach for a three-phase cascaded multilevel inverter (CMLI) for a grid-connected PV system is proposed in this paper. The photovoltaic (PV) is connected to CMLI isolated DC-connections based on the respective DC-to-DC converters. The proposed hybrid method is the joint performance of white shark optimizer (WSO) and extended fuzzy wavelet neural network (FWNN); thus, it is known as the WSO-FWNN method. The primary objective of the proposed method is to regulate the power or increase the energy conversion of solar systems and to maintain the power quality. CMLI is incorporated switches, diodes and sources that are modelled to obtain the optimal control signal with the proposed controller. WSO produces the most optimal control signal data set from the CMLI and evaluates the gain parameter under the source's current normal value. FWNN is performed, which forecasts the most optimal control signals from the CMLI using the data set produced by the WSO. The variation of the system parameters and the external disturbance is reduced with the proposed method, and it satisfies the load demand of the system. At last, the proposed approach is actualized on the MATLAB/Simulink platform, and its performance is compared with existing methods. From the simulation outcome, the proposed approach shows less switching power losses of 0.04 W and a THD of 2.51%.*

Keywords *- Cascaded multilevel inverter, DC to DC converters, photovoltaic, THD, Power Quality.*

1. Introduction

Infiltration into Renewable Energy Sources (RES) has increased exponentially due to increased demand for global electricity and awareness of the environmental problems caused by the widespread use of fossil fuels [1]. One of the RES is a photovoltaic (PV) source utilized to tackle energy problems worldwide, particularly in areas with high levels of sunlight [2]. At present, it is used to join the grid highly. Indeed, its grid connection form is very efficient due to the guarantee for the distribution of local loads and transmits the excess PV-generated electricity to the grid [3]. Due to the sudden growth of power electronics and system approaches, the use of solar and wind systems connected to the grid has increased significantly [4]. The components such as rectifiers, boost converters and inverters play an essential role in achieving effective power conversion based on RES [5]. There are various disturbances occur in the grid due to the utilization of various types of inverters and nonlinear loads [6]. Usually, high heat is generated due to the harmonic of the gird current, which causes an increase in losses and insulation breakdown [7]. It produces the torque ripple, leading to motor vibrations and noises. Moreover, unnecessary reactive power leads to power factor reduction and produces losses [8]. Additionally, failures, as well as neutral current, are created by an unbalanced current [9].

Therefore, the PV system does not exceed harmonic content limits and reactive current [51]. To reduce the harmonics and minimizes the loss, multilevel inverters are introduced, which are highly suited for medium and high-power conversion systems [11-12].

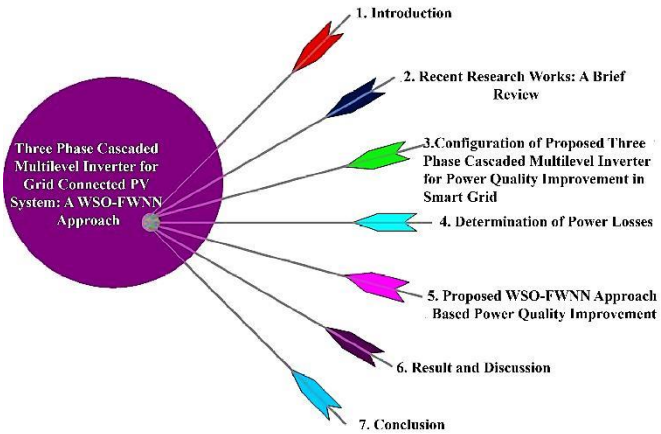

Fig. 1 Configuration of proposed work

Currently highly preferred DC to AC converter configuration is the multi-level inverter (MLI) topology, as they have extra advantages [54].MLI is characterized by the

ability to manage high voltages and good noise reduction, excellent electromagnetic compatibility, and the low-pressure voltage across switches. [14-15].RES grid integration uses a number of conventional symmetric, asymmetric and optimal characteristics [52]. Problems like voltage variations, harmonic production, flickering and unbalanced DC connection capacitor voltages occur in the hybrid wind-solar system, affecting power quality [17]. Also, some unnecessary harmonics are produced because of the power converters. The hybrid wind-solar system produces energy based on the sun's radiation and the wind's speed [18]. But the output voltage is fluctuated because of the variable wind speed and power generation or voltage difference. The maximum DC current in the DC capacitor connection varies depending on the variation of the DC connection capacitor voltages [19]. Therefore, to control the DC connection voltage in the grid-integrated system, MLI topologies are connected [20].

A hybrid approach to the cascaded multilevel inverter (CMLI) for the grid-connected PV system. The photovoltaic (PV) is connected to CMLI isolated DC-connections based on the respective DC-to-DC converters. The proposed hybrid method is the joint performance of white shark optimizer (WSO) and extended fuzzy wavelet neural network (FWNN); thus, it is known as the WSO-FWNN method. The major objective of the proposed method is to regulate the power or increase the energy conversion of solar systems. The organization of the proposed work is illustrated in fig 1.

2. Recent Research Work: A Brief Review

Previously, there have been several research works in the literature that are based on multilevel inverters for the grid-connected system with several methods and features. Some of them revised as follows, Multilevel 3-phase voltage source inverter (VSI) for PV system was described by V. F. Pireset al. [21]. Three-phase, two-level VSI isolation transformer was utilized in the introduced system. The photovoltaic panels were attached to the DC side of every three-phase VSI. The open-end winding of the three-phase isolation transformer was connected to the AC side of every three-phase VSI to guarantee the various stages. The PWM was utilized to modulate the VSI hybrid modulation approach suggested by A. Ahmad and P. Samuel [55] to implement the balancing of self-boost capable of multilevel inverter using capacitor voltage of PV. The cascaded and neutral-point-clamped topologies were different for harmonics analysis. The RFCSA control approach was suggested by R. Ramya and T. S. Sivakumaran [23].

Enhancing the PV system's efficiency and extracting the PV's maximal power was the major contribution of the introduced approach. Voltages, current, power, and modulation index were considered the input parameter of the system. QZSI managed the interface between the PV dc source and load. The introduced approach was controlling the dc link voltage, current and minimization of injected power. An operational impact of a Distribution Static Compensator (D-STATCOM) and Unified Power Quality Conditioner (UPQC) into a cascaded H-bridge Nine-Level Multi-Level Inverter (NL:MLI) was illustrated by A. Gupta [24]. The introduced approach performance was evaluated based on the DC voltage and two PV modules. The power quality was analysed based on faulted conditions at linear load.

The introduced approach calculates the Total Harmonic Distortion (THD) and DC offset current. Cascaded Transformer dependent Modular Multilevel Inverter (CTMLI) for PV systems have been suggested by Ahmed et al. [53]. The introduced system utilized the three full-bridge (FB) circuits for switching the input DC voltage. CTMLI cost was minimized by utilising the transformer turn ratio and cost estimation model. To increase the maximum power and control the voltage and current of the PV system, M K Das et al. [26] have suggested a multi-level inverter. The minimum number of switches was considered, and dc voltage was derived by correctly connecting PV to the inverter. The suggested novel approach controls the voltage, and the current controller provides the maximal power of the system. The hybridisation of both colour harmony algorithm (CHA), as well as extreme gradient boosting (XGBOOST) for grid-connected hybrid systems, including CMLI, was developed by V. T.V. Mahendiran [27]. CMLI was operated based on the gain parameter tuning of the proposed controller. CHA was utilized to evaluate the gain parameter, and XGBOOST was used to obtain the control parameters.

2.1. Background of Research Work

The electric grid not only generation, transmission, and distribution but also relates to manufacturers and service providers. With its public and private domains, the electricity office improves energy transfer to access reliable, secure, clean energy. Smart grid technologies are made possible by two-way communication technologies, control systems, and computer processing. The recent review based on power quality improvement of PV with MLI system reveals that power quality is a significant contributing factor. The MLI's recent developments are mostly focused on enhancing power quality and reducing the number of switches. The problems based on power quality are the challengeable ones for installing the control design. Due to fluctuation of voltage and problems based on safety provides issue in the utility grid and reduces the reliability and quality of power. MLI is utilized to overcome these issues. Various types of MLIs topologies, such as diode-clamped multilevel inverters (DCMLI), cascaded multilevel inverters (CMLI), and so on, have been utilized recently. Various approaches are utilized to solve the issue of power quality of PV systems with MLI. The fuzzy logic controller needs a number of data. It is no more feasible for programs lesser or greater than historical data. The major disadvantages of the genetic algorithm are

very sluggish processing and the inability to recognize the optimal solution. The main research gaps identified are that very few control approaches were suggested in the literature for optimally controlling the grid-connected PV system. Still, the suggested approaches are ineffective in reducing power losses and total harmonic reduction. These problems stimulated me to do this research work.

3. Configuration of Proposed Three-Phase Cascaded Multilevel Inverter for Power Quality Improvement in Smart Grid

Three-Phase CMLI for Grid Connected PV System is illustrated in fig 2 (a). Considered the level of CMLI is 9, which is connected among the source and load. The PV system, connected to the boost converter, extracts the maximum power. The proposed approach is to control the voltage and current and decrease the system's harmonics. The proposed method is utilized to provide the control signal and is connected to the PWM [28-31]. Using the PWM pulses, the gate driver provides the switching pulse of the MLI. The hybrid WSO-FWNN approach is proposed to reduce the harmonics of the system. The WSO is utilized to produce the control signal of the system, and the FWNN is utilized to predict the optimal control signal. The structure of the proposed 9-level inverter is illustrated in fig 2 (b).

3.1. Multilevel Inverter Model

The multilevel inverter executes power conversion on multiple voltage steps, achieving better power quality and greater voltage capacity [32-35]. The MLI is composed of a multi-level bridge topology serial connection. The general output voltage of MLI is,

$$v_{o/p} = v^1_{o/p} + v^2_{o/p} + \cdots v^n_{o/p} \quad (1)$$

The number of the voltage level of the inverter is described by,

$$Ns=2n+1 \quad (2)$$

The maximal output voltage of n level inverter is,

$$v^{\max}_{out} = n * v_{dc} \quad (3)$$

The quantity of voltage steps for n level inverter is provided as,

$$\text{For } j = 1,2,\ldots n,\ N_s = \begin{cases} 2^{n+1}-1 \ if\ v_j = 2^{j-1}v_{dc} \\ 3^n \quad if\ v_j = 3^{j-1}v_{dc} \end{cases} \quad (4)$$

The maximum output voltages of these n level inverters are written as,

$$\text{For } j = 1,2,\ldots n,$$

$$V^{\max}_{out} = \begin{cases} (2^n - 1)v_{dc} & if\ v_j = 2^{j-1}v_{dc} \\ \left(\frac{3^n - 1}{2}\right) v_{dc} & if\ v_j = 3^{j-1}v_{dc} \end{cases} \quad (5)$$

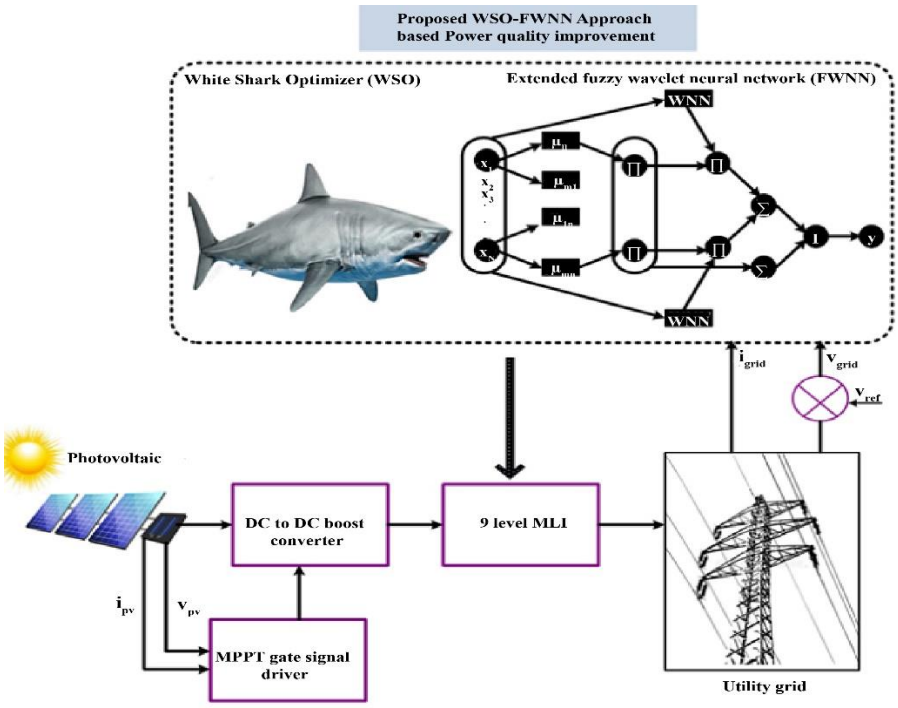

Fig. 2(a) Configuration of the proposed three-Phase CMLI for Grid Connected PV System

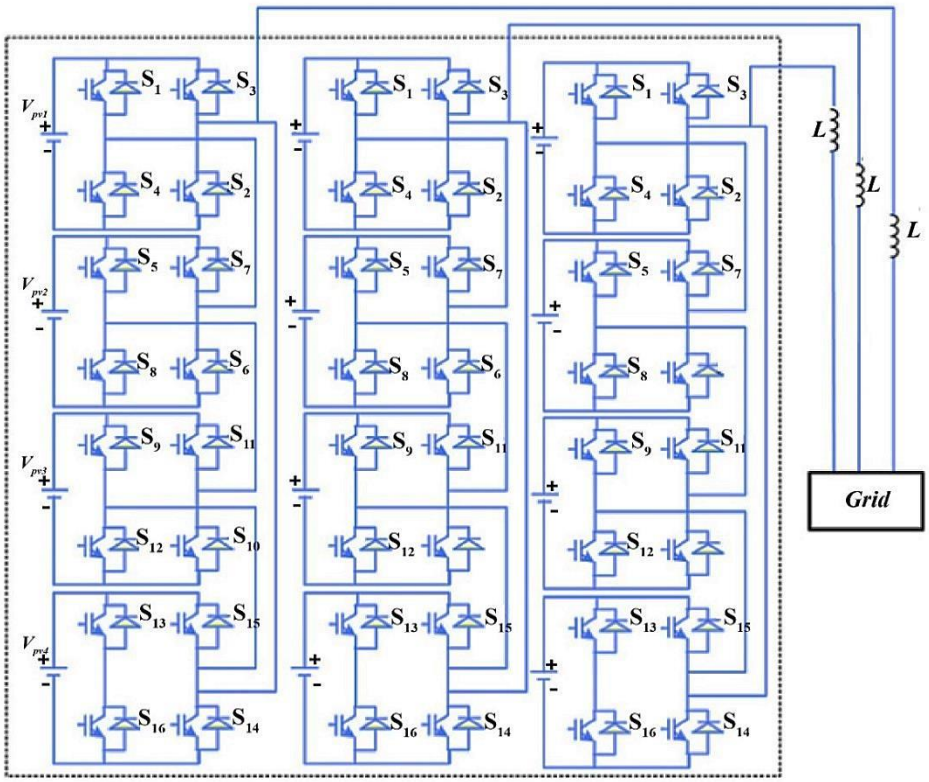

Fig. 2 (b) Structure of the proposed 9-level inverter

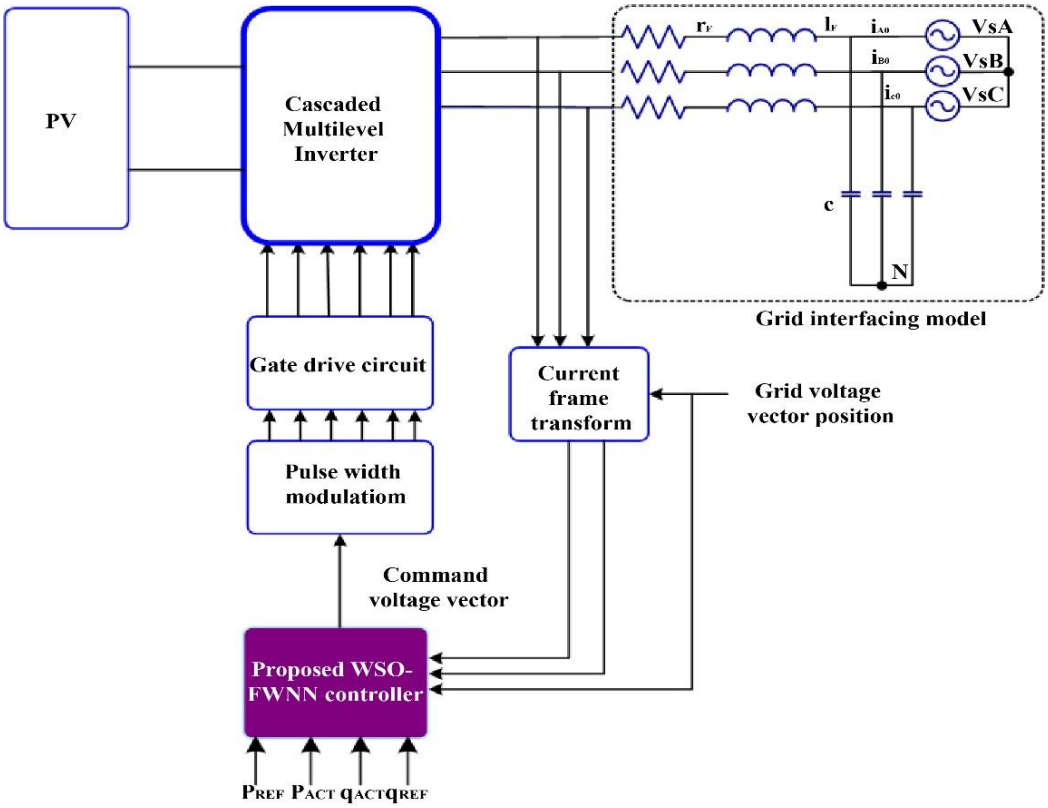

Fig. 3 Proposed CMLI with grid connection

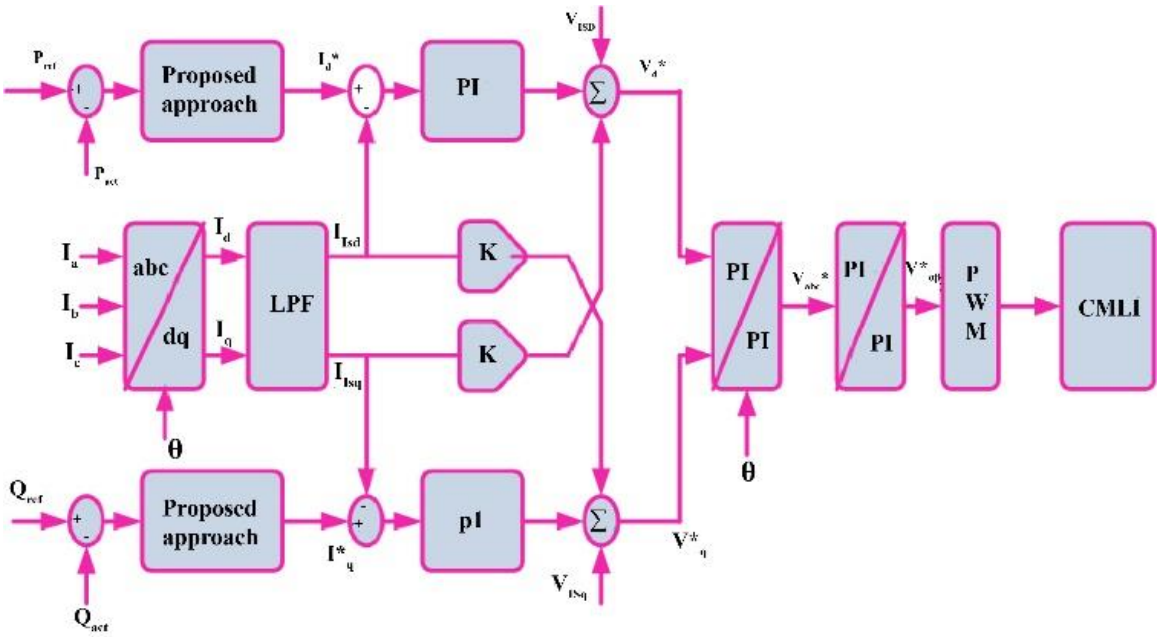

Fig. 4 Active and reactive control action with dq control architecture

3.2. Modelling of CMLI With Grid Connection

The proposed CMLI with grid connection is displayed in fig 3. The state space model [36] of the proposed system is expressed by,

$$\frac{d}{dt}\begin{bmatrix} i_a \\ i_b \\ i_c \end{bmatrix} = \frac{r_{lum}}{l_{lum}}\begin{bmatrix} i_a \\ i_b \\ i_c \end{bmatrix} + \frac{1}{l_{lum}}\left(\begin{bmatrix} v_{sa} \\ v_{sb} \\ v_{sc} \end{bmatrix} - \begin{bmatrix} v_a \\ v_b \\ v_c \end{bmatrix}\right) \quad (6)$$

Eqn (16) is modified by the Park's transformation. Then it is described by,

$$\frac{d}{dt}\begin{bmatrix} i_D \\ i_Q \end{bmatrix} = \begin{bmatrix} -\frac{r_{lum}}{l_{lum}} & f_{ang} \\ -f_{ang} & -\frac{r_{lum}}{l_{lum}} \end{bmatrix}\begin{bmatrix} i_D \\ i_Q \end{bmatrix} + \frac{1}{l_l}\left(\begin{bmatrix} v_{sD} \\ v_{sQ} \end{bmatrix} - \begin{bmatrix} v_D \\ v_Q \end{bmatrix}\right) \quad (7)$$

Here, r_{lum} as lumped resistance, l_{lum} as lumped inductance, the grid voltage is denoted as V_s, direct and quadrature axis current is denoted as i_D, i_Q. The two-quadrant signals are obtained from the three-phase original signals described in equations (15) and (16).

3.3. Modeling of Active and Reactive Control for Grid-Connected PV System

The three-phase grid current is passed to the proposed approach to generate the essential reference voltage and current. The grid voltage, current, and reference current are converted from abc to dq reference frame and then the dq [36-37] components are passed through the PI controller, which is tuned by the proposed approach and delivers the control signals. By using PWM, the switching signal of CMLI is generated. The active and reactive control action with dq control architecture is displayed in fig 4.

3.4. Voltage and Current Harmonic Distortion

Due to passive as well as active nonlinear devices, the power system produces harmonics. Total voltage harmonic distortion and total current harmonic distortion are used to determine the harmonic performance of the bus system [54]. The ratio of the sum of the power of the entire harmonic voltage components to the power of the essential voltage frequency is called total voltage harmonic distortion.

$$TVHD = \frac{100 \times \sqrt{v_{rms}^2 - v_{frms}^2}}{v_{frms}} \quad (8)$$

$$TIHD = \frac{100 \times \sqrt{i_{rms}^2 - i_{frms}^2}}{i_{frms}} \quad (9)$$

Here, TVHD denotes total voltage harmonic distortion, TIHD denotes total current harmonic distortion, v_{frms} denotes fundamental voltage frequency, i_{frms} denotes fundamental current frequency, v_{rms} denotes harmonic voltage component, i_{rms} denotes harmonic current component.

4. Determination of Power Losses

The power losses reduce the system's efficiency; hence the reduction of losses is necessary. In power electronic devices, there are two kinds of losses, conduction and switching losses [39-41].

4.1 Switching Power Losses

The amount of electrical energy reduced during the switching time of the tested object is called switching power loss. It is classified into turn-on and turn-off losses. These losses affect the switching frequency, the gate drive circuit's resistance, the input voltage's magnitude, and the junction temperature. The switching power losses are detected by,

$$P_{SW}^{ON} = \frac{1}{t}\int_0^{T_{ON}} v_{SW}(T)\, i(T) dT \tag{10}$$

$$P_{SW}^{OFF} = \frac{1}{t}\int_0^{T_{OFF}} v_{SW}(T)\, i(T) dT \tag{11}$$

Here, the time interval taken by the switch for on and off is denoted as T_{ON}, T_{OFF}. The voltage and current of the switch is $v_{SW}(T)$,$i(T)$. The total loss is described by the addition of on and off losses which are described by,

$$P_{SW} = \sum_{j=1}^{m}\left[\sum_{k=1}^{n_{on}} P_{SW,j}^{ON} + \sum_{k=1}^{n_{off}} P_{SW,j}^{OFF}\right] \tag{12}$$

Here, total switching power losses are denoted as P_{sw}, and the number of the switching devices is denoted as m. This loss occurs when the system works on or without load.

4.2. Conduction Losses

Under load conditions, the running time loss occurs, which decreases system performance during operation based on load current and input voltage. For Both the switches and the diodes, conduction loss is calculated. The conduction loss based on the diode is calculated by,

$$P_{CL}^{D} = \frac{1}{t}\int_o^t v_T^f\, i_T^f d_T^d dT \tag{13}$$

Here, diode conduction losses is denoted as P_{CL}^{D}, forward voltage and the diode's current is denoted as v_T^f, i_T^frespectively, and the duty cycle of the diode is denoted as d_T^d.

$$P_{CL}^{SW} = \frac{1}{t}\int_o^t v_T^{ce}\, i_T^c d_T^{SW} dT \tag{14}$$

Here, switch conduction losses are denoted as P_{CL}^{SW}, conduction voltage and the switch's current is denoted as v_T^{CE}, i_T^c, the duty cycle of the switch is denoted as d_T^{SW}. The addition of switching and diode conduction loss is described by,

$$P_{CL} = \sum_{j=1}^{m} P_{CL,j}^{D} + P_{CL,j}^{SW} \tag{15}$$

The total loss of the proposed system is determined by the addition of conduction losses and switching power losses which are described by,

$$P_{Losses} = P_{CL} + P_{SW} \tag{16}$$

5. Proposed WSO-FWNN Approach-Based Power Quality Improvement

The hybrid WSO-FWNN approach is proposed to improve the power quality of the smart grid system. Here considered, the PV was the source and utilized the cascaded multilevel inverter for reducing the harmonics [42-43]. The proposed method reduces the variation of a system parameter and the disturbance on external, satisfying the load demand of the system. The detailed description of the proposed method is described as follows,

5.1. WSO Approach-Based Generation of Control Signal

The WSO approach is inspired based on the white sharks' characteristics, like exceptional senses of hearing and smell. These characteristics achieve the balancing of the exploration and exploitation of WSO [44]. Thus, it enables search agents to explore every possible area of search space for optimization. The search agents of the WSO provide the solution based on the randomly updated position. It extensively searches the food in the depths of the ocean. Three characteristics are utilized to find the prey: Moving towards the prey based on the reluctance of the waves caused by the movement of the prey, the random search for prey in the ocean depths, and shark behavior in finding nearby prey. The step-by-step method of the WSO approach is described as follows,

Step 1: Initialization

The input population of the shark-like load current, dc-link voltage, PV voltage, PI controller gain parameters, constraints, iteration of the system

Step 2: Random generation

Randomly create the initialized parameter on the matrix form *Y*

$$= \begin{bmatrix} (I_{lo}, v_{DC}, v_{PV}, K_p, K_i)^{11} & \cdots & \cdots & (I_{lo}, v_{DC}, v_{PV}, K_p, K_i)^{1N} \\ (I_{lo}, v_{DC}, v_{PV}, K_p, K_i)^{21} & \cdots & \cdots & (I_{lo}, v_{DC}, v_{PV}, K_p, K_i)^{2N} \\ \vdots & \vdots & \vdots & \vdots \\ (I_{lo}, v_{DC}, v_{PV}, K_p, K_i)^{m1} & \cdots & \cdots & (I_{lo}, v_{DC}, v_{PV}, K_p, K_i)^{MN} \end{bmatrix} \tag{17}$$

Step 3: Fitness Evaluation

The fitness is evaluated depends upon objective function, which is described by,

$$F = MIN(THD) \tag{18}$$

Step 4: Movement speed towards prey

The movement speed towards prey is based on the characteristics like hearing, sight and smell. In this step, based on prey movement, if the prey is moved, then it hears that and moves towards the prey. The equation for the movement is described by,

$$V = [N \times R(1, N)] + 1 \tag{19}$$

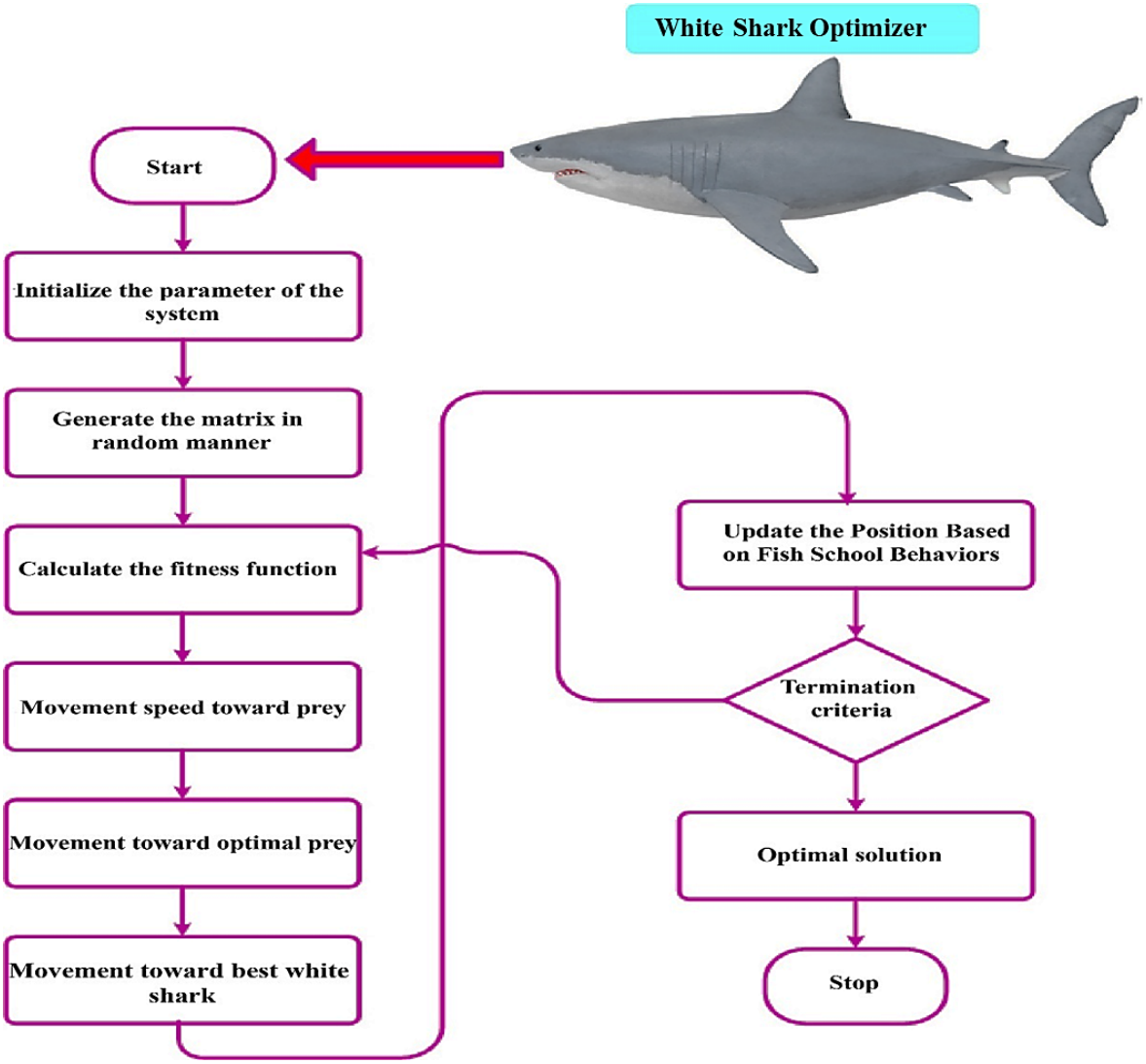

Fig. 5 Flowchart of proposed WSO approach

Here, the vector of random numbers is denoted as$R(1, N)$. The force of shark is described by,

$$p = p^{MAX} + (p^{MAX} - p^{MIN}) \times e^{-(4j/J)^2} \quad (20)$$

Here, the current and maximum number of iterations is denoted asj, J, and initial and subordinate velocities are represented as$p^{MAX}\ p^{MIN}$.

Step 5: Movement towards Optimal Prey

The movement towards the optimal prey is described by,

$$W_{j+1}^{I} = \begin{cases} W_j^I . \chi \oplus W_o + U.A + l.B; R < strength \\ W_j^I + v_j^I / F; R \geq strength \end{cases} \quad (21)$$

the negative operator is denoted as χ; one-dimensional binary vectors are denoted asA, B; lower and upper limits of search space are denoted as l, U, the logical vector is denoted as W_o.

Step 6: Movement towards Best White Shark

The best white shark is determined based on the nearest distance of the shark close to prey which is described by,

$$\bar{W}_{j+1}^{`I} = W_{BEST}^{G} + R_1 d_W \, sgn(R_2 - 0.5) \quad (22)$$

Step 7: Update the Position Based on Fish School Behaviors

Preserved the position of best white shark prey and updated all other fish positions, which are described by,

$$W_{j+1}^{`I} = \frac{W_j^{`I} + \bar{W}_{j+1}^{`I}}{2R} \quad (23)$$

The final position of large white sharks (i.e., search agents) is the search location closest to the optimal prey.

Step 8: Termination Criteria

Check the termination criteria, and if the optimal outcome is obtained, then the process ends; otherwise, go to step 3. The flowchart of the proposed WSO method is displayed in fig 5.

5.2. Prediction Of Control Signal Based On Extended Fuzzy Wavelet Neural Network

In this algorithm, the signal processing, neural network and fuzzy logic using the decomposition wavelets, which deal with the dynamic systems and learning process, is performed by the neural network (NN). WNN improves the mapping interface amid inputs and outputs in a network. The complicated nonlinear process operation performed by fuzzy technology is incomplete, and factors are uncertain. Hence it provides a satisfactory performance using the structure of FWNN, as shown in fig 6.

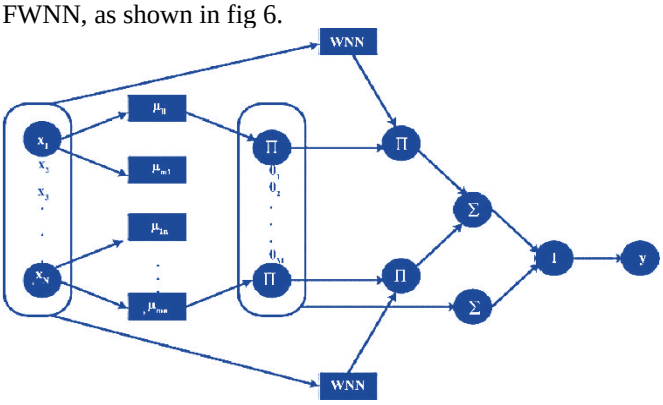

Fig. 6 Structure of the FWNN

Moreover, based on fuzzy technology, the experts' knowledge is limited to creating IF-Then rules and these problematic situations are performed by NN. Therefore, here to predict the optimal gain parameter, FWNN is proposed. The rapid training speed trains FWNN, and it is possible to analyze the nonlinear objects. The parameters of PV are used by the fuzzification while determining the input-to-output maps by wavelet, through which the accuracy is increased. By using translation and delay, the parameters are adjusted by FWNN [45-47]. The FWNN approach consists of 7 layers which are described as,

5.2.1. Layer 1

It accepts the input and sends that to the next layer. Here consider the input variable as x_S and the output variable is y_S.

5.2.2. Layer 2

Fuzzification layer is known as layer 2. This layer process the membership function. It associates the input crisp valuex_J with the fuzzy set using membership degree $(M_{KJ}(x_J))$.

5.2.3. Layer 3

In the third layers, every node has a fuzzy rule, and the outcome is determined by,

$$O_k^{Lay3} = \prod_{J=1}^{N} \mu_{kJ}(x_J), k = 1,2,..m \quad (24)$$

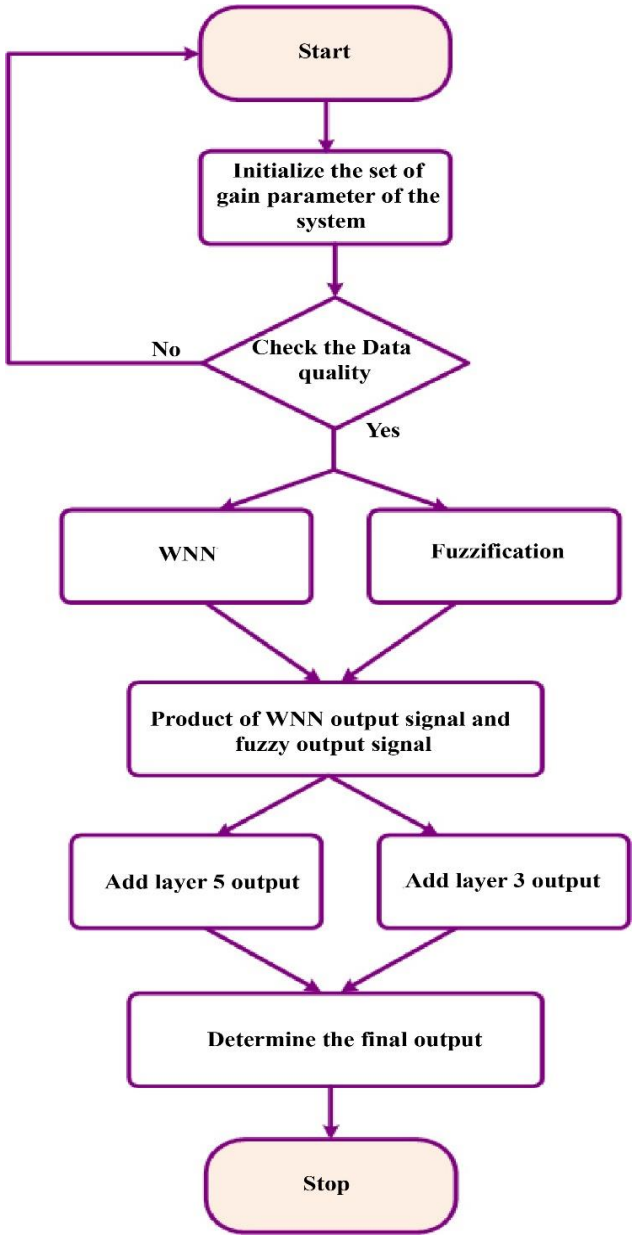

Fig. 7 Flow chart of the proposed FWNN approach

Here, a subset of input signals is denoted as$J$,$k$representing the subset of fuzzy rule, and membership degree is denoted asμ_{kJ}.

5.2.4. Layer 4

In this layer, permit the much number of neural networks that accept the input variable as$X_1..X_N$. The outcome of the fourth layer is determined by,

$$O_k^{Lay4} = \sum_{I=1}^{n_K} w_I^k \phi_I^k + \bar{y}_k \quad (25)$$

5.2.5. Layer 5

The fuzzy interference system is utilized by layers 5 to 7, which are incorporated into fuzzification components, fuzzy inference motor and defuzzification. The outcome of layer 5 is described by,

$$O_k^{Lay5} = O_k^{Lay3}.O_k^{Lay4} = O_k y_k \quad (26)$$

5.2.6. Layer 6

The layer six outputs are defined by,

$$O_1^{Lay6} = \sum_{k=1}^{m} O_k^{Lay5}.O_2^{Lay6} = \sum_{k=1}^{m} O_k^{Lay3} \quad (27)$$

5.2.7. Layer 7

Layer 7 is the output node; it provides the final output, which is described by,

$$y = O_k^{Lay7} = \frac{O_1^{Lay6}}{O_2^{Lay6}} = \frac{\sum_{k=1}^{m} O_k y_k}{\sum_{k=1}^{m} O_k} \quad (28)$$

Fig 7 shows the flowchart of the proposed FWNN approach.

6. Results and Discussion

The performance of the proposed approach depends on simulation results. WSO-FWNN approach is proposed to enhance the power quality of the system. The cascaded multilevel inverter (CMLI) is utilized to reduce the harmonics of the system. CMLI is incorporated into less number of switches, diodes and sources that are modelled to obtain the optimal control signal with the proposed controller.

The proposed method is actualized in the MATLAB/Simulink platform, and its performance is related to existing approaches. The proposed approach is analyzed on three conditions: normal load condition, linear load irradiation and temperature change, and nonlinear load irradiation and Temperature Change. Here, parameters like voltage, current, active and reactive power, irradiation and temperature are investigated to determine the system's performance. Adaptive Neuro-Fuzzy Interference System (ANFIS), Mayfly Optimization Algorithm (MFA), and Side-Blotched Lizard Algorithm (SBLA) are utilized to compare the proposed approach performance.

6.1. Case 1: Performance Analysis of Proposed Approach Based on Normal Load Condition

Figure 8 represents the analysis of irradiation under normal loading conditions. It is known from the graph that the irradiation is 1000 W/m^2. Analysis of temperature analysis during normal loading conditions is illustrated in figure 9, which shows that the temperature value is 25 degrees Celsius. Figure 10 depicts the PV current and voltage graph in which the current value is initially increased from 150 A to 340 A and then drops to 15 A at 0.05 time/ sec during the remaining time period. The current value stays constant at 15 A. Figure 11 illustrates the analysis of dc voltage, inverter, and load voltage. Here, during the time interval of 0 to 0.05 time/ sec, the dc voltage increases from 0 to 180 V, and it remains constant for the remaining time period. The inverter voltage varies from -600 to 600 V, which is figure 11 (b), and the load voltage is displayed in figure 11 (c). It is shown that the load voltage varies from -100 to 100V in the time duration of 0 to 0.05 times/ sec, and for the remaining time period, it differs from -400 to 400 with a slight deviation. The modulation voltage is shown in figure 10, where the voltage waveform initially increases from 0 to 50 V and then it drops to -200 V, again increases to 300 V and drops to -380 V, and again rises to 380V during the time interval of 0 to 0.05 time/ sec. The voltage value continuously varies for the remaining time duration from -380 to 380 V.

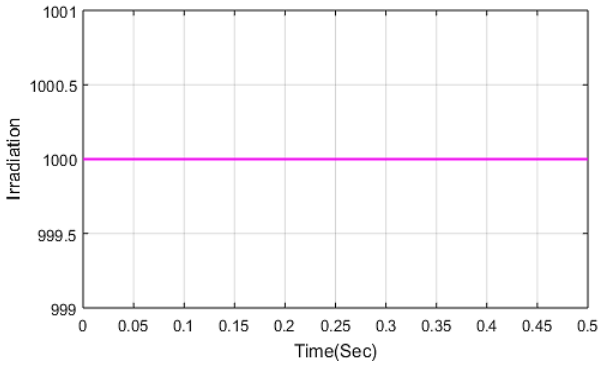

Fig. 8 Analysis of irradiation under normal loading conditions

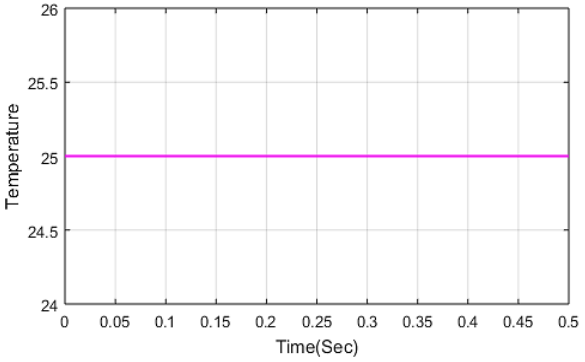

Fig. 9 Analysis of temperature under normal loading conditions

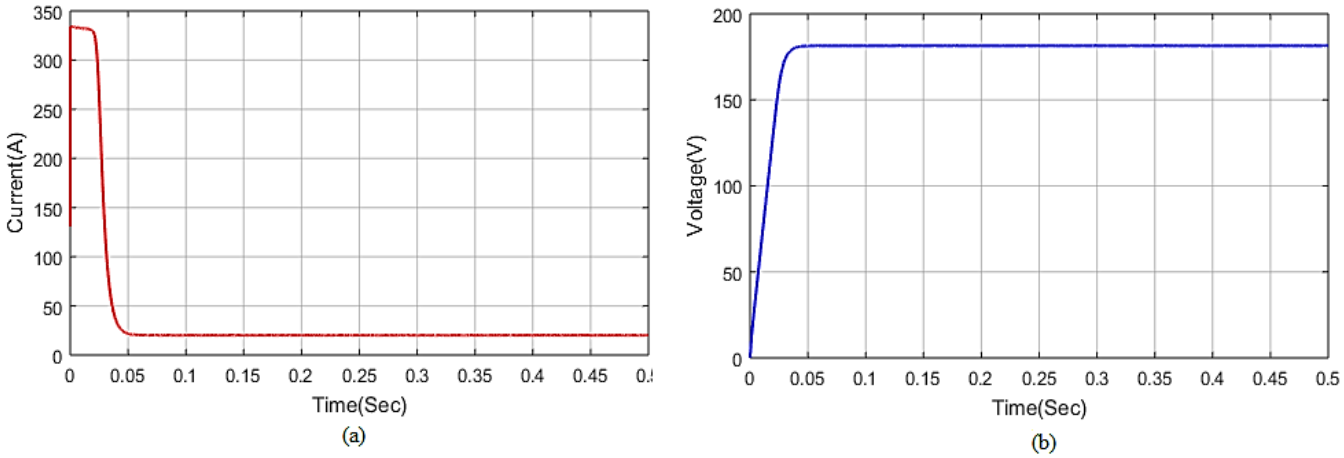

Fig. 10 Case 1 -Analysis of PV in (a) Current (b) Voltage

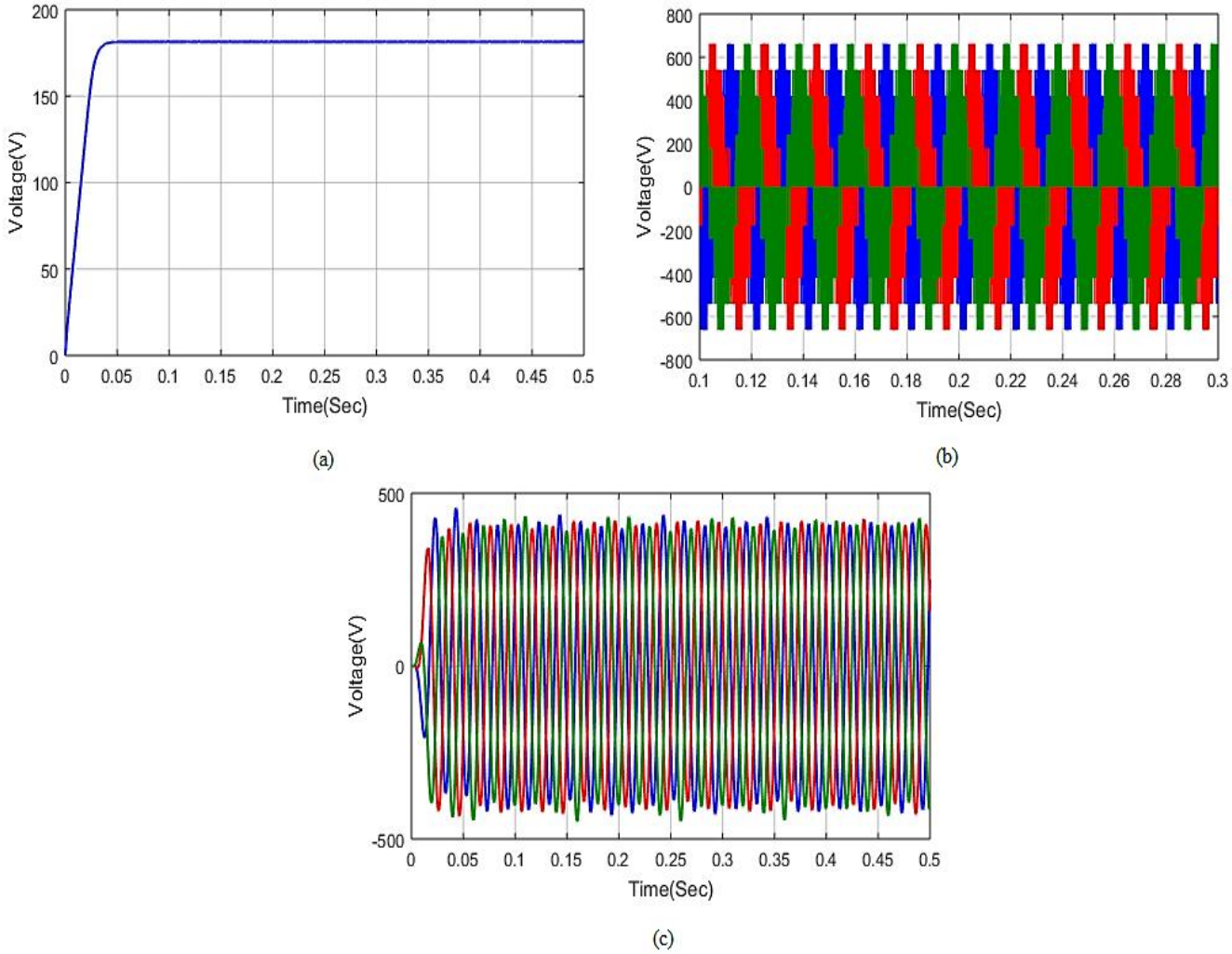

Fig. 11 Case 1-Analysis of (a) DC voltage, (b) Inverter voltage, (c) Load voltage

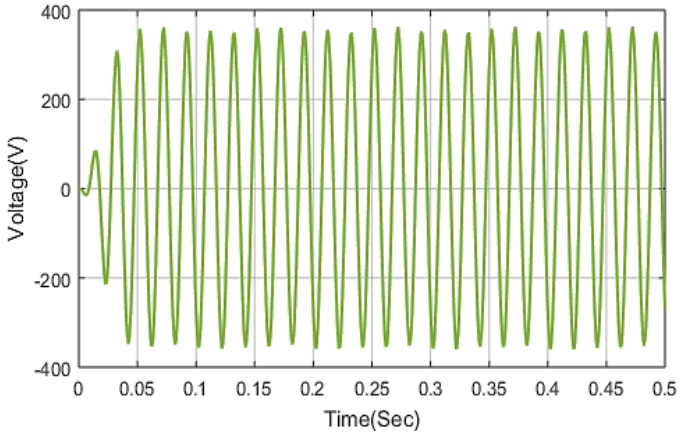

Fig. 12 Case 1 -Analysis of Modulation voltage

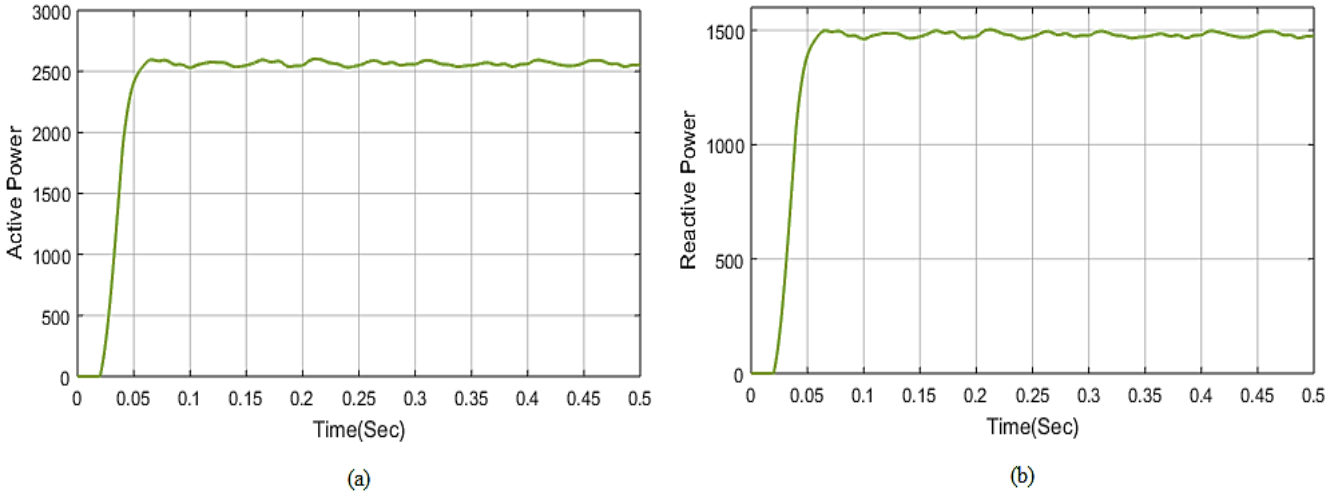

Fig. 13 Case 1 -Analysis of (a) Load active power (b) Load reactive power

Load active and reactive power analysis under normal loading conditions is displayed in figure 13. The active load power is initially 0, and it increases to 2500 KW during the time interval of 0.025 to 0.05 time/sec. Its leftovers are stable at 2500 kW with slight variation, shown in figure 13 (a). Likewise, the reactive load power increases from 0 to 1500 kW in the time period of 0.025 to 0.05 times/ sec. Then it remains constant at the same value with a slight deviation.

6.2. Case 2: Performance Analysis of Proposed Approach Based On Linear Load Irradiation and Temperature Change Condition

Figure 14 represents the analysis of irradiation under linear loading conditions. It is known from the graph that the irradiation is 700 W/m^2 for the time period of 0 to 0.2 times/sec, then it rises to 900 W/m^2 and remains stable during the time duration of 0.2 to 0.4 times/ sec. Again, it emerges to 1000 W/m^2 and stays constant for the remaining time duration. Analysis of temperature during linear loading conditions is illustrated in figure 15, and it shows that the temperature value is 20 degrees Celsius for the time period of 0 to 0.25 time/ sec, and it increases to 25 degrees Celsius. For the remaining time period, it remains constant at 25 degrees Celsius. Figure 10 depicts the PV current and voltage graph in which the current value initially increases from 100 A to 240 A, then drops to 15 A at 0.05 time/ sec. For the remaining time period, the current value stays constant at 15 A with a slight deviation at the time of 0.2 time/ sec and 0.4 time /sec, which is detected and optimized by the proposed technique. The PV voltage shown in figure 16 (b) emerges from 0 to 195 V in the time interval of 0 to 0.2 times/ sec. It gradually increases to 196 V at the interval of 0.2 to 0.4 time/ sec, then emerges to 197 V and remains constant for the remaining time period.

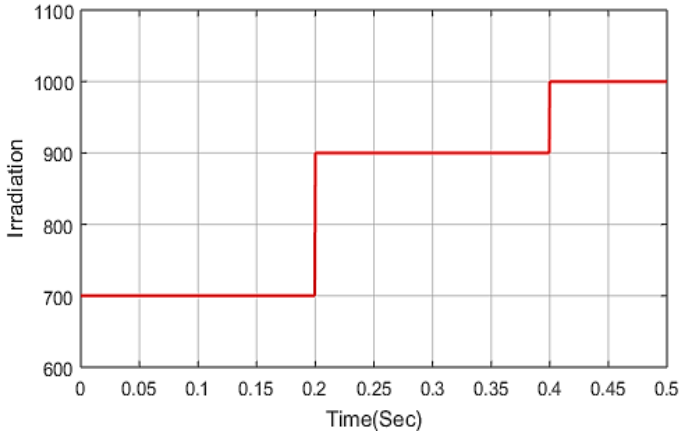

Fig. 14 Analysis of irradiation under linear loading condition

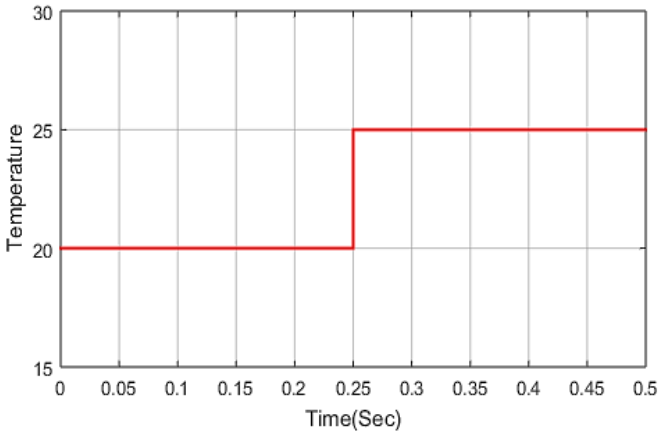

Fig. 15 Analysis of temperature under linear loading condition

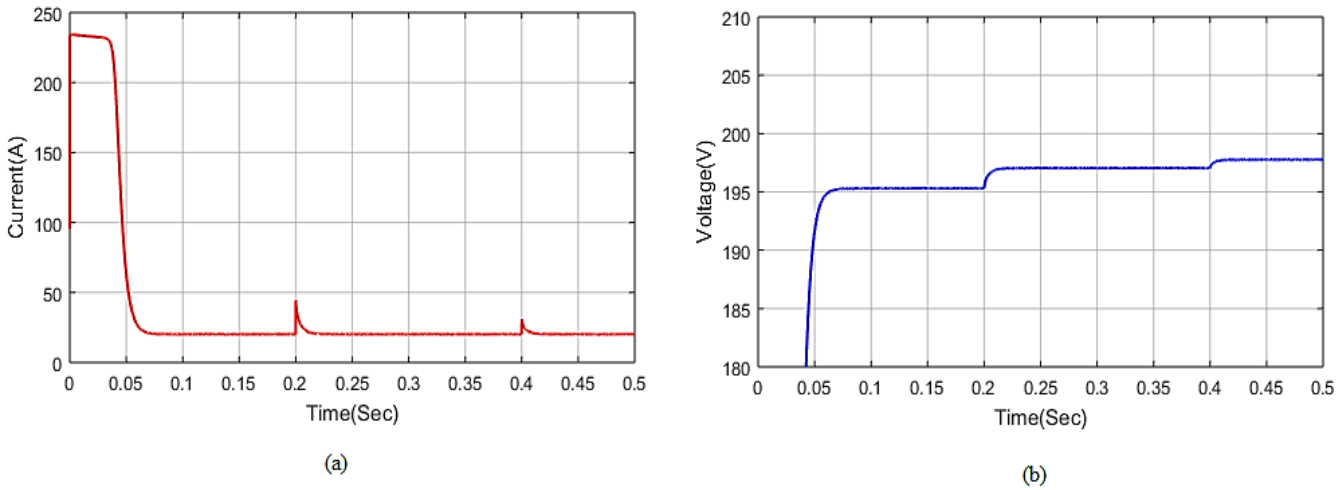

Fig. 16 Case 2 -Analysis of PV (a) Current (b) Voltage

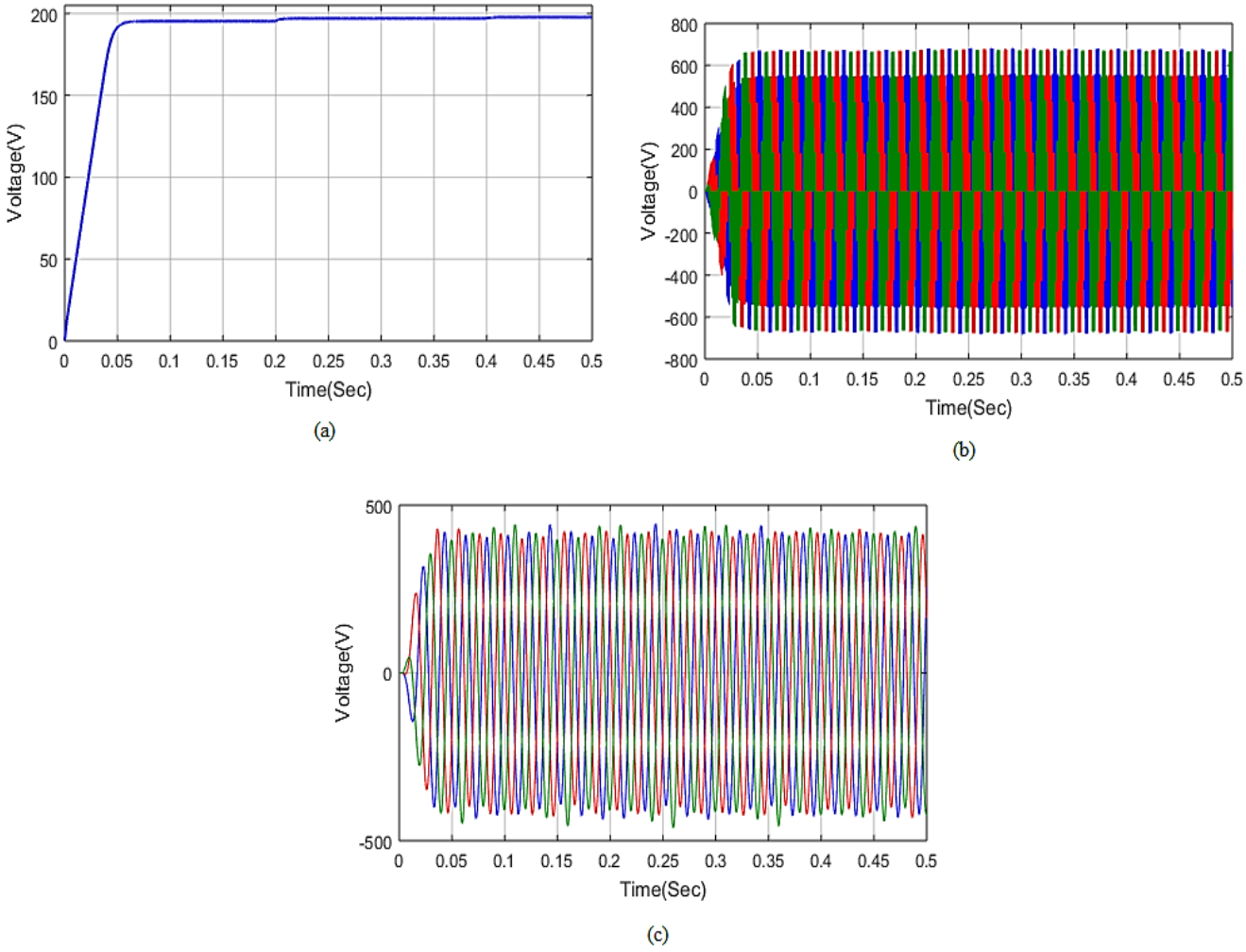

Fig. 17 Case 2 -Analysis of (a) DC voltage, (b) Inverter voltage, (c) Load voltage

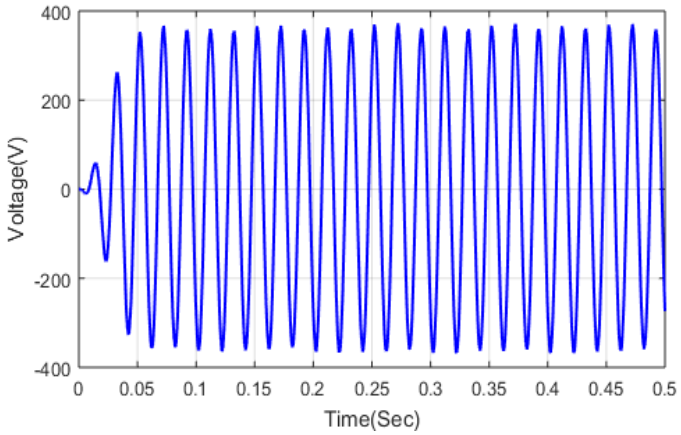

Fig. 18 Case 2 -Analysis of Modulation voltage

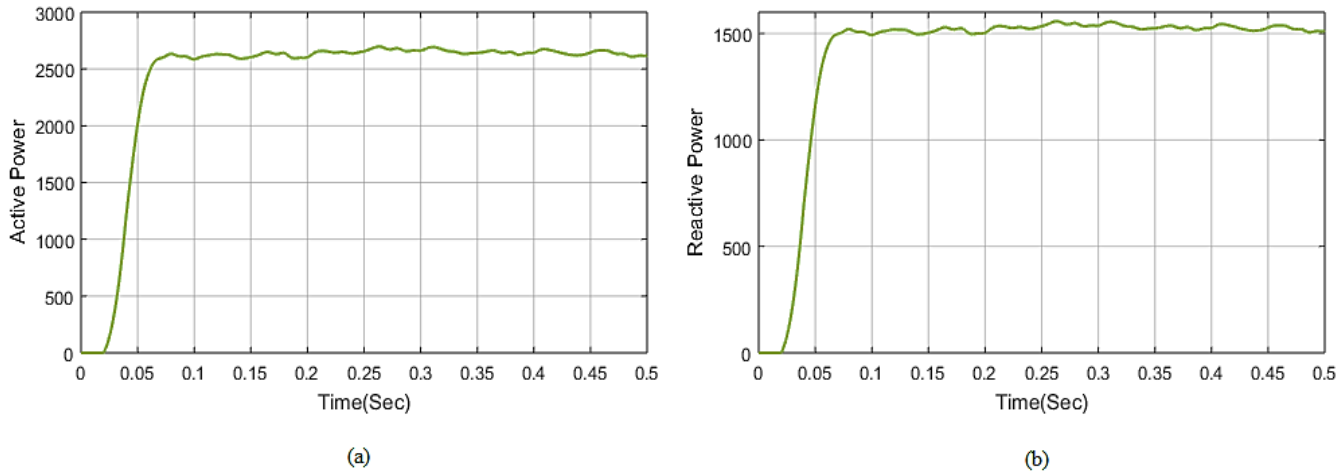

Fig. 19 Case 2 -Analysis of (a) Load active power (b) Load reactive power

Figure 17 illustrates the analysis of dc voltage, inverter, and load voltage under linear loading conditions. Here, during the time interval of 0 to 0.05 time/ sec, the dc voltage increases from 0 to 190 V, and it remains constant for the remaining time period. The inverter voltage is maximized from 0 to 600 at 0 to 0.05 time/ sec. Then, it varies from -600 to 600 V, shown in figure 17 (b), and the load voltage is displayed in figure 17 (c). It is shown that the load voltage is highly distorted due to linear loading conditions in the time interval of 0 to 0.05 time/ sec, and it continues to vary from -100 to 100V for the remaining time period. The modulation voltage under linear loading conditions is shown in figure 18. During the time interval of 0 to 0.05 time/ sec, the voltage waveform initially increases from 0 to 50 V, then drops to -150 V; again, it increases to 250 V and drops to -300 V; besides, it rises to 350V. The voltage value continuously varies for the remaining time duration from -350 to 350 V. The analysis of Load active and reactive power under linear loading conditions is displayed in figure 19. The dynamic load power is initially 0, and it increases to 2600 KW during the time interval of 0.025 to 0.075 time/sec. It remains constant at 2600 kW with slight variation for the remaining time period, shown in figure 13 (a). Similarly, the reactive load power increases from 0 to 1500 kW in the time period of 0.025 to 0.075 times/sec. Then it remains constant at the same value with slight deviation for the remaining time duration.

6.3. Case 3: Performance Analysis of Proposed Approach Based on Nonlinear Load Irradiation and Temperature Change Condition

Figure 20 represents the analysis of irradiation under nonlinear loading conditions. It is known from the graph that the irradiation is 700 W/m^2 for the time period of 0 to 0.2 times/sec, then it rises to 900 W/m^2 and remains stable during the time duration of 0.2 to 0.4 times/ sec. Again, it emerges to 1000 W/m^2 and stays constant for the remaining time duration. Analysis of temperature during nonlinear loading conditions is illustrated in figure 21, and it shows that the temperature value is 20 degrees Celsius for the time period of 0 to 0.25 time/ sec, and it increases to 25 degrees Celsius. For the remaining time period, it remains constant at 25 degrees Celsius. Figure 22 depicts the PV current and voltage graph in which the current value initially increases from 100A to 240A and then drops to 20A at 0.05 time/ sec. For the remaining time period, the present value stays constant at 20 A. A slight deviation is encountered at the time of 0.2 times/ sec and 0.4 times /sec, which are detected and optimized by the proposed technique. The PV voltage shown in figure 22 (b) emerges from 0 to 195V in the time interval of 0 to 0.05 times/ sec. It gradually increases to 196V at the time of 0.2 time/ sec, and then it emerges to 197V and remains constant for the remaining time period. Figure 23 illustrates the analysis of dc voltage, inverter, and load voltage under nonlinear loading conditions. Here, during the time interval of 0 to 0.05 time/ sec, the dc voltage increases from 0 to 190V, and it remains constant for the remaining time period. Then, it is highly distorted due to nonlinear load and varies from -600 to 600 V, shown in figure 23 (b), and the load voltage is displayed in figure 23 (c). It is shown that the load voltage is highly deviated due to linear loading conditions, and it continues to vary from -100 to 100V for the remaining time period. The modulation voltage under nonlinear loading conditions is shown in figure 24. During the time interval of 0 to 0.05 time/ sec, the voltage waveform initially increases from 0 to 50 V, then drops to -150 V; again, it increases to 250 V and drops to -320 V; again, it rises to 350V. The voltage value continuously varies for the remaining time duration from -350 to 350 V.

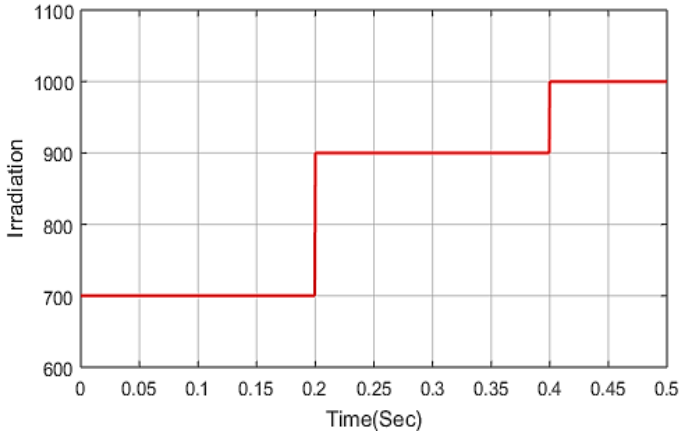

Fig. 20 Analysis of irradiation under nonlinear loading condition

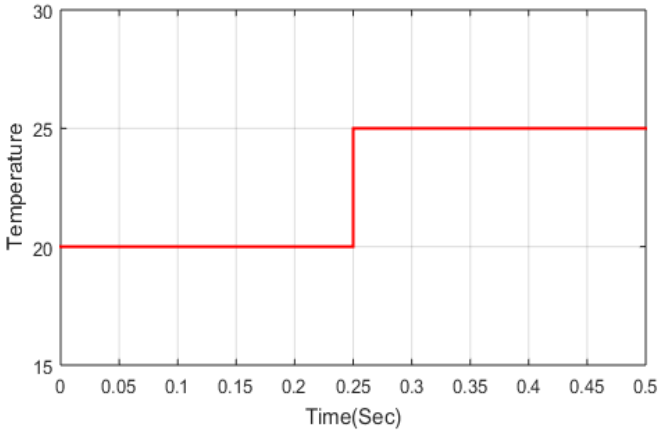

Fig. 21 Analysis of temperature under nonlinear loading condition

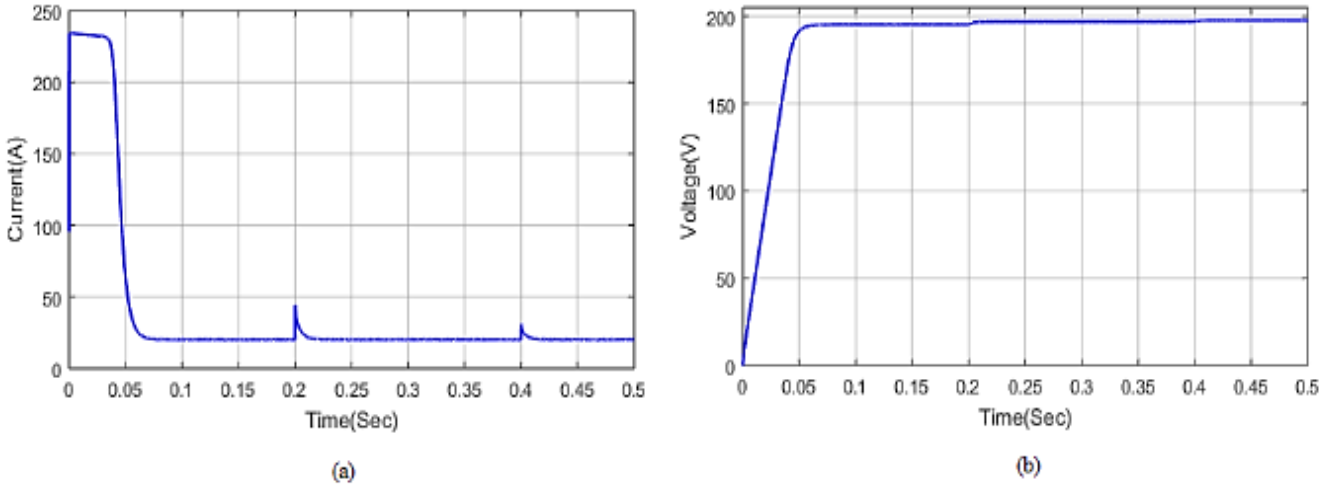

Fig. 22 Case 3 -Analysis of PV (a) Current (b) Voltage

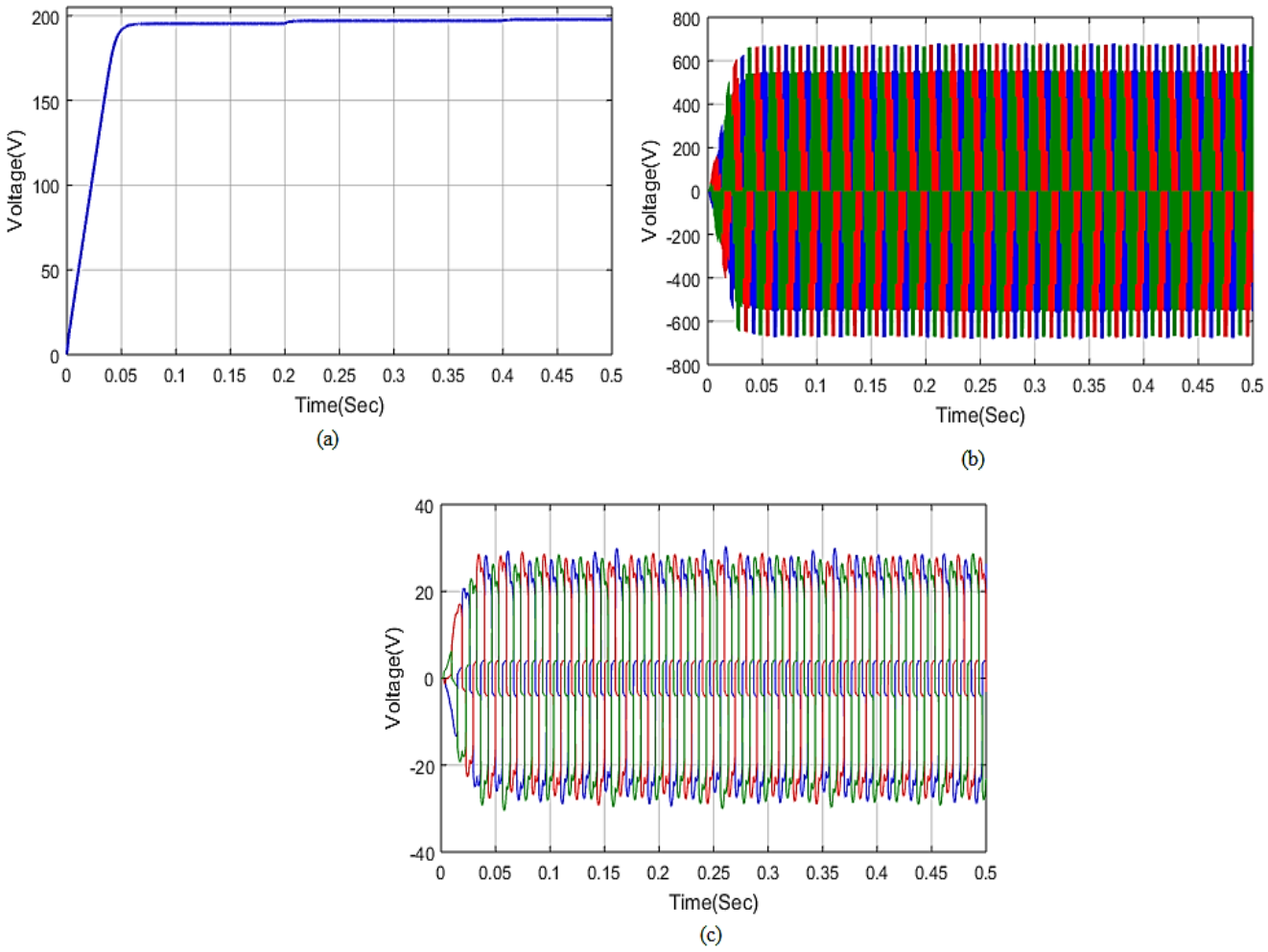

Fig. 23 Case 3 -Analysis of (a) DC voltage, (b) Inverter voltage, (c) Load voltage

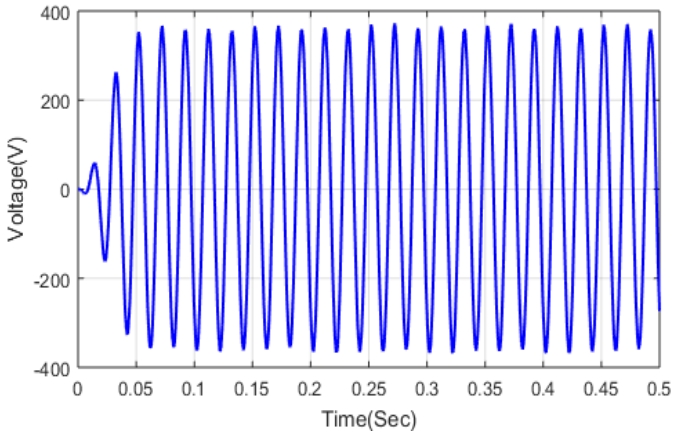

Fig. 24 Case 3 -Analysis of Modulation voltage

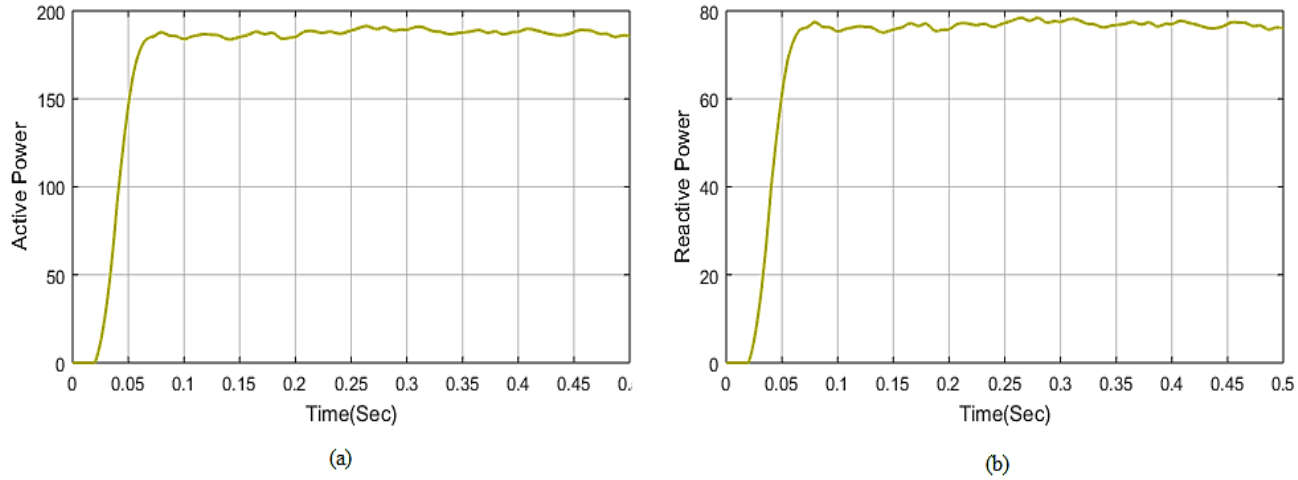

Fig. 25 Case 3 -Analysis of (a) Load active power (b) Load reactive power

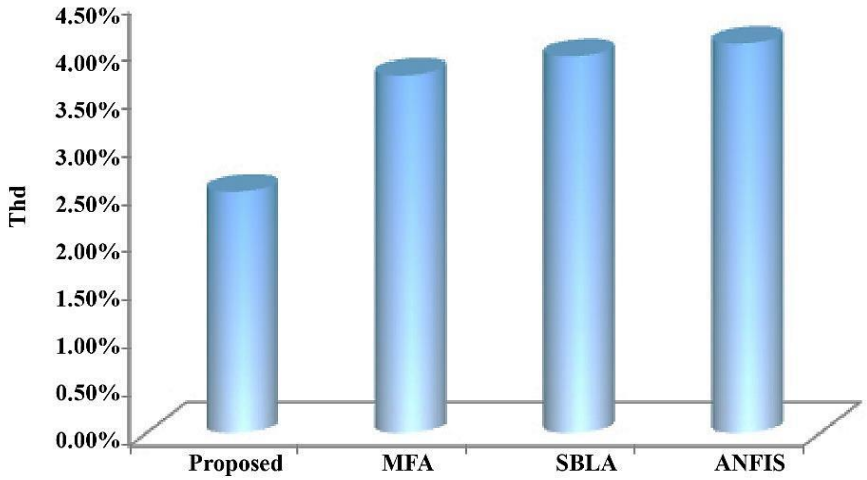

Fig. 26 Comparison of THD of proposed and existing approach

The analysis of Load active and reactive power under nonlinear loading conditions is displayed in figure 25. The active load power is initially 0, and it increases to 190 KW during the time interval of 0.025 to 0.075 time/sec. It remains constant at 190 kW with slight variation for the remaining time period, shown in figure 25 (a). Similarly, the reactive load power increases from 0 to 90 kW in the time period of 0.025 to 0.075 times/sec. Then it remains constant at the same value with slight deviation for the remaining time duration. A comparison of THD of the proposed and existing approach is fig 26. The proposed approach THD is 2.51%, and the existing approaches like ANFIS, MFA and SBLA THD become 4.05 %, 3.72 % and 3.92 %, respectively. From this comparison, it is concluded that the proposed approach provides fewer harmonics than the existing one.

Table 1 tabulated the comparative analysis of conduction and switching losses of the proposed and existing approach. The proposed approach-based CMLI provides 7.9 W conduction loss and 0.04 W switching losses. The existing approach provides high losses than the proposed one. It reveals that the proposed approach is best one than the existing approach.

Table 1. Comparative Analysis Based on Losses Proposed and Existing Approach

Solution Approach	Conduction power losses	Switching power losses
Proposed	7.9 W	0.04 W
MFA	8.9W	0.06W
SBLA	9.5W	0.08W
ANFIS	10.1W	0.1W

7. Conclusion

An efficient hybrid WSO-FWNN approach is proposed in this paper to increase the power quality of grid-connected PV systems. The proposed system is incorporated with a cascaded multilevel inverter which is utilized to reduce the harmonics of the system. CMLI is incorporated into less number of switches, diodes and sources that are modelled to obtain the optimal control signal with the proposed controller. The WSO approach is utilized to generate the control signal of the CMLI, and the FWNN approach optimally predicts that control signal. The proposed approach is actualized on the MATLAB/Simulink platform, and its performance is related to existing approaches like ANFIS, MFA and SBLA. The proposed method is analyzed in three conditions: normal load condition, linear load irradiation, temperature change and nonlinear load irradiation, and temperature change. Here, parameters like voltage, current, active and reactive power, irradiation and temperature are investigated to determine the system's efficiency. From the simulation obtained, the THD of the proposed approach is 2.51%, and the existing approaches like ANFIS, MFA and SBLA THD become 4.05 %, 3.72 % and 3.92 %, respectively. The conduction and switching losses are analyzed for proposed and existing approaches. The proposed approach provides less loss than the existing one is proved.

References

[1] Licheng Wang et al., "Real-Time Coordinated Voltage Control of PV Inverters and Energy Storage for Weak Networks with High PV Penetration," *IEEE Transactions on Power Systems*, vol. 33, no. 3, pp. 3383-3395, 2018. *Crossref*, http://doi.org/10.1109/TPWRS.2018.2789897

[2] Houshang Salimian, and Hossein Iman-Eini, "Fault-Tolerant Operation of Three-Phase Cascaded H-Bridge Converters Using an Auxiliary Module," *IEEE Transactions on Industrial Electronics*, vol. 64, no. 2, pp. 1018-1027, 2017. *Crossref*, http://doi.org/10.1109/TIE.2016.2613983

[3] Xiaoming Zha et al., "Segmented Power Distribution Control System Based on Hybrid Cascaded Multilevel Converter with Parts of Energy Storage," *IET Power Electronics*, vol. 10, no. 15, pp. 2076-2084, 2017. *Crossref*, https://doi.org/10.1049/iet-pel.2016.0943

[4] Md Mubashwar Hasan et al., "A New Cascaded Multilevel Inverter Topology with Galvanic Isolation," *IEEE Transactions on Industry Applications*, vol. 54, no. 4, pp. 3463-3472, 2018. *Crossref*, https://doi.org/10.1109/TIA.2018.2818061

[5] P. Ponnambalam et al., "Fuzzy Controlled Switched Capacitor Boost Inverter," *Energy Procedia*, vol. 117, pp. 909-916, 2017. *Crossref*, https://doi.org/10.1016/j.egypro.2017.05.210

[6] Yashwant Sawle, S.C. Gupta, and Aashish Kumar Bohre, "Socio-Techno-Economic Design of Hybrid Renewable Energy System Using Optimization Techniques," *Renewable Energy*, vol. 119, pp. 459-472, 2018. *Crossref*, https://doi.org/10.1016/j.renene.2017.11.058

[7] Pandurangan Shanthi, Govindarajan Uma, and Muniyandi Selvanathan Keerthana, "Effective Power Transfer Scheme for a Grid Connected Hybrid Wind/Photovoltaic System," *IET Renewable Power Generation*, vol. 11, no. 7, pp. 1005-1017, 2017. *Crossref*, https://doi.org/10.1049/iet-rpg.2016.0592

[8] Fatemeh Shahnazian et al., "Interfacing Modular Multilevel Converters for Grid Integration of Renewable Energy Sources," *Electric Power Systems Research*, vol. 160, pp. 439-449, 2018. *Crossref*, https://doi.org/10.1016/j.epsr.2018.03.014

[9] Tom Wanjekeche, "Modeling, Control and Experimental Investigation of a Cascaded Hybrid Modular Inverter for Grid Interface Application," *IEEE Access*, vol. 6, pp. 21296-21313, 2018. *Crossref*, https://doi.org/10.1109/ACCESS.2018.2822403

[10] Mr. Anem Apparo, and Dr. G. Chandra Sekhar, "A Grid Connected HRES using Seven Level Inverter - A Hybrid MFO-RBFNN Technique," *International Journal of Engineering Trends and Technology*, vol. 68, no. 7, pp. 56-68, 2020. *Crossref*, https://doi.org/10.14445/22315381/IJETT-V68I7P209S

[11] Babkrani Youssef et al., "Selective-Harmonic Elimination with an Optimized Multicarrier Modulation Techniques for Cascaded H-Bridge Multilevel Inverter," *Journal of Applied Mathematics and Computation*, vol. 3, no. 1, pp. 574-582, 2019. *Crossref*, https://doi.org/10.26855/jamc.2019.01.001

[12] K. D. E. Kerrouche et al., "Fractional-Order Sliding Mode Control for D-STATCOM Connected Wind Farm Based DFIG Under Voltage Unbalanced," *Arabian Journal for Science and Engineering*, vol. 44, no. 3, pp. 2265-2280, 2019. *Crossref*, https://doi.org/10.1007/s13369-018-3412-y

[13] J. Shirishan et al., "Deep Learning-Based Image Processing Approach for Irradiance Estimation in MPPT Control of Photovoltaic Applications," *SSRG International Journal of Electrical and Electronics Engineering*, vol. 9, no. 9, pp. 32-37, 2022. *Crossref*, https://doi.org/10.14445/23488379/IJEEE-V9I9P104

[14] Ali Mortezaei et al., "Multifunctional Control Strategy for Asymmetrical Cascaded H-Bridge Inverter in Microgrid Applications," *IEEE Transactions on Industry Applications*, vol. 53, no. 2, pp. 1538-1551, 2017. *Crossref*, https://doi.org/10.1109/TIA.2016.2627521

[15] Hugues Renaudineau et al., "A PSO-Based Global MPPT Technique for Distributed PV Power Generation," *IEEE Transactions on Industrial Electronics*, vol. 62, no. 2, pp. 1047-1058, 2015. *Crossref*, https://doi.org/10.1109/TIE.2014.2336600

[16] John Nweke, Arthur Ekwue, and Emenike Ejiogu, "Economic Feasibility of Integrating Solar Photovoltaic Distributed Generation with Nigerian Power System," *International Journal of Recent Engineering Science*, vol. 7, no. 3, pp. 61-71, 2020.

[17] Fabio Viola, "Experimental Evaluation of the Performance of a Three-Phase Five-Level Cascaded H-Bridge Inverter by Means FPGA-Based Control Board for Grid Connected Applications," *Energies*, vol. 11, no. 12, p. 3298, 2018. *Crossref*, https://doi.org/https://doi.org/10.3390/en11123298

[18] Roman Kosenko et al., "Comparative Analysis of Semiconductor Power Losses of Galvanically Isolated Quasi-Z-Source and Full-Bridge Boost DC-DC Converters," *Electrical, Control and Communication Engineering*, vol. 8, no. 1, pp. 5-12, 2015. *Crossref*, https://doi.org/10.1515/ecce-2015-0001

[19] Yushan Liu et al., "An Effective Control Method for Three-Phase Quasi-Z-Source Cascaded Multilevel Inverter Based Grid-Tie Photovoltaic Power System," *IEEE Transactions on Industrial Electronics*, vol. 61, no. 12, pp. 6794-6802, 2014. *Crossref*, https://doi.org/10.1109/TIE.2014.2316256

[20] Javier Pórtoles, Camino González, and Javier M. Moguerza, "Electricity Price Forecasting with Dynamic Trees: A Benchmark Against the Random Forest Approach," *Energies*, vol. 11, no. 6, p. 1588, 2018. *Crossref*, https://doi.org/10.3390/en11061588

[21] V. Fernão Pires et al., "Three-Phase Multilevel Inverter for Grid-Connected Distributed Photovoltaic Systems Based in Three Three-Phase Two-Level Inverters," *Solar Energy*, vol. 174, pp. 1026-1034, 2018. *Crossref*, https://doi.org/10.1016/j.solener.2018.09.083

[22] M. Usharani et al., "An Optimized Deep Learning Model Based PV Fault Classification for Reliable Power Generation," *SSRG International Journal of Electrical and Electronics Engineering*, vol. 9, no. 9, pp. 23-31, 2022. *Crossref*, https://doi.org/10.14445/23488379/IJEEE-V9I9P103

[23] Rajendran Ramya, and Thangavel Swaminathan Sivakuaran, "An Efficient RFCSA Control Strategy for PV Connected Quasi-Z-Source Cascaded Multilevel Inverter (QZS-CMI) System," *International Journal of Numerical Modelling: Electronic Networks, Devices and Fields*, vol. 33, no. 1, 2019. *Crossref*, https://doi.org/10.1002/jnm.2660

[24] Akhil Gupta, "Power Quality Evaluation of Photovoltaic Grid Interfaced Cascaded H-Bridge Nine-Level Multilevel Inverter Systems Using D-STATCOM and UPQC," *Energy*, vol. 238, p. 121707, 2022. *Crossref*, https://doi.org/10.1016/j.energy.2021.121707

[25] Obayuwana A, and Igbonoba E.E.C, "Design and Implementation of a Smart Prepaid Solar Inverter System," *International Journal of Recent Engineering Science*, vol. 7, no. 4, pp. 7-13, 2020. *Crossref*, https://doi.org/ 10.14445/23497157/IJRES-V7I4P102

[26] Madan Kumar Das, Kartick Chandra Jana, and Akanksha Sinha, "Performance Evaluation of an Asymmetrical Reduced Switched Multi-Level Inverter for a Grid-Connected PV System," *IET Renewable Power Generation*, vol. 12, no. 2, pp. 252-263, 2017. *Crossref*, https://doi.org/10.1049/iet-rpg.2016.0895

[27] T.V.Mahendiran, "A Color Harmony Algorithm and Extreme Gradient Boosting Control Topology to Cascaded Multilevel Inverter for Grid Connected Wind and Photovoltaic Generation Subsystems," *Solar Energy*, vol. 211, pp. 633-653, 2020. *Crossref*, https://doi.org/10.1016/j.solener.2020.09.079

[28] Zhao Liu et al., "A Power Distribution Control Strategy between Energy Storage Elements and Capacitors for Cascaded Multilevel Inverter with Hybrid Energy Sources," *IEEE Access*, vol. 7, pp. 16880-16891, 2019. *Crossref*, https://doi.org/10.1109/ACCESS.2019.2895675

[29] Bhupender Sharma, Ratna Dahiya, and Jayaram Nakka, "Effective Grid Connected Power Injection Scheme Using Multilevel Inverter-Based Hybrid Wind Solar Energy Conversion System," *Electric Power Systems Research*, vol. 171, pp. 1-14, 2019. *Crossref*, https://doi.org/10.1016/j.epsr.2019.01.044

[30] Buddhadeva Sahooa, Sangram Keshari Routray, and Pravat Kumar Rout, "Repetitive Control and Cascaded Multilevel Inverter with Integrated Hybrid Active Filter Capability for Wind Energy Conversion System," *Engineering Science and Technology, An International Journal*, vol. 22, no. 3, pp. 811-826, 2019. *Crossref*, https://doi.org/10.1016/j.jestch.2019.01.001

[31] Rajesh Vasu et al., "Three-Phase Trinary Asymmetric Multilevel Inverter with Single DC Source and Open-Loop Control," *IEEE Open Journal of Industry Applications*, vol. 2, pp. 259-277, 2021. *Crossref*, https://doi.org/10.1109/OJIA.2021.3105605

[32] S. Satish Kumar, and M. Sasi Kumar, "Intelligent Hybrid Technique for Cascaded Multilevel Inverter Based Three Phase Grid-Tie Hybrid Power System: A WPSNN Technique," *Journal of Ambient Intelligence and Humanized Computing*, vol. 12, no. 10, pp. 9637-9666, 2021. *Crossref*, https://doi.org/10.1007/s12652-020-02707-3

[33] Jingrong Yu et al., "Simplified SVPWM-Based Soc Balancing Strategy for Three-Phase Cascaded H-Bridge Multilevel Converter in Off-Grid Energy Storage Systems," *International Journal of Electrical Power & Energy Systems*, vol. 137, p. 107474, 2022. *Crossref*, https://doi.org/10.1016/j.ijepes.2021.107474

[34] P. Meenalochini, and E. Sakthivel, "An Efficient GBDTRSO Control Strategy for PV Connected H-Bridge Nine Level MLI System with Quasi-Z-Source Inverter," *Applied Soft Computing*, vol. 113, p. 108026, 2021. *Crossref*, https://doi.org/10.1016/j.asoc.2021.108026

[35] Ozan Gulbudak, and Mustafa Gokdag, "Finite Control Set Model Predictive Control Approach of Nine Switch Inverter-Based Drive Systems: Design, Analysis, and Validation," *ISA Transactions*, 2021. *Crossref*, https://doi.org/10.1016/j.isatra.2020.10.037

[36] Junfeng Liu et al., "A Novel Nine-Level Inverter Employing One Voltage Source and Reduced Components as High-Frequency AC Power Source," *IEEE Transactions on Power Electronics*, vol. 32, no. 4, pp. 2939-2947, 2017. *Crossref*, https://doi.org/10.1109/TPEL.2016.2582206

[37] Hossein Khoun Jahan, Kazem Zare, and Mehdi Abapour, "Verification of a Low Component Nine-Level Cascaded-Transformer Multilevel Inverter in Grid-Tied Mode," *IEEE Journal of Emerging and Selected Topics in Power Electronics*, vol. 6, no. 1, pp. 429-440, 2018. *Crossref*, https://doi.org/10.1109/JESTPE.2017.2772323

[38] CH Venkata Ramesh, and A Manjunatha, "A Bi-LSTM and GRU Hybrid Neural Network with BERT Feature Extraction for Amazon Textual Review Analysis," *International Journal of Engineering Trends and Technology*, vol. 70, no. 5, pp. 131-144, 2022. *Crossref*, https://doi.org/10.14445/22315381/IJETT-V70I5P215

[39] Kartick Chandra Jana, Sujit K. Biswas, and Suparna KarChowdhury, "Dual Reference Phase Shifted Pulse Width Modulation Technique for a N -Level Inverter-Based Grid Connected Solar Photovoltaic System," *IET Renewable Power Generation*, vol. 10, no. 7, pp. 928-935, 2016. *Crossref*, https://doi.org/10.1049/iet-rpg.2015.0393

[40] N. Sandeep, and Udaykumar R. Yaragatti, "Operation and Control of an Improved Hybrid Nine-Level Inverter," *IEEE Transactions on Industry Applications*, vol. 53, no. 6, pp. 5676-5686, 2017. *Crossref*, https://doi.org/10.1109/TIA.2017.2737406

[41] Bhupender Sharma, Ratna Dahiya, and Jayaram Nakka, "Effective Grid Connected Power Injection Scheme Using Multilevel Inverter-Based Hybrid Wind Solar Energy Conversion System," *Electric Power Systems Research*, vol. 171, pp. 1-14, 2019. *Crossref*, https://doi.org/10.1016/j.epsr.2019.01.044

[42] Peeyush Kala, and Sudha Arora, "Implementation of Hybrid GSA SHE Technique in Hybrid Nine-Level Inverter Topology," *IEEE Journal of Emerging and Selected Topics in Power Electronics*, vol. 9, no. 1, pp. 1064-1074, 2021. *Crossref*, https://doi.org/10.1109/JESTPE.2019.2963239

[43] Malik Braik et al., "White Shark Optimizer: A Novel Bio-Inspired Meta-Heuristic Algorithm for Global Optimization Problems," *Knowledge-Based Systems*, vol. 243, p. 108457, 2022. *Crossref*, https://doi.org/10.1016/j.knosys.2022.108457

[44] Saeid Jafarzadeh Ghoushchi et al., "An Extended New Approach for Forecasting Short-Term Wind Power Using Modified Fuzzy Wavelet Neural Network: A Case Study in Wind Power Plant," *Energy*, vol. 223, p. 120052, 2021. *Crossref*, https://doi.org/10.1016/j.energy.2021.120052

[45] Adil Sarwar et al., "A Nine-Level Cascaded Multilevel Inverter with Reduced Switch Count and Lower Harmonics," *Lecture Notes in Electrical Engineering*, pp. 723-738, 2019. *Crossref*, https://doi.org/10.1007/978-981-13-6772-4_62

[46] Ratna Rahul Tupakula, "A Generalized Single-Phase Cascaded Multilevel Inverter with Reduced Switch Count," *Electrical Engineering*, vol. 103, no. 2, pp. 1115-1125, 2020. *Crossref*, https://doi.org/10.1007/s00202-020-01141-0

[47] Dr. C.B. Venkataramanan, and Pranesh V, "Hybrid Multilevel Inverter with Reduced Switches and Harmonics," *SSRG International Journal of Electrical and Electronics Engineering*, vol. 3, no. 3, pp. 10-15, 2016. *Crossref*, https://doi.org/10.14445/23488379/IJEEE-V3I3P102

[48] Pairote Thongprasri, "An Investigation of THD in 5-level NPC Multilevel Inverter Based on Multicarrier PWM Techniques," *SSRG International Journal of Electrical and Electronics Engineering*, vol. 4, no. 8, pp. 20-28, 2017. *Crossref*, https://doi.org/10.14445/23488379/IJEEE-V4I8P104

[49] E. Shravan, and Dr. R. Arul Murugan, "Survey on Multilevel Inverter with Less Number of Switches for Different Loads," *SSRG International Journal of Electrical and Electronics Engineering*, vol. 5, no. 6, pp. 16-25, 2018. *Crossref*, https://doi.org/10.14445/23488379/IJEEE-V5I6P104

[50] V.Jamuna Venkatesan, and Gayathrimonicka Subarnan, "Multi Carrier based Multilevel Inverter with Minimal Harmonic Distortion," *International Journal of Power Electronics and Drive Systems*, vol. 6, no. 2, pp. 356-361, 2015. *Crossref*, http://doi.org/10.11591/ijpeds.v6.i2.pp356-361

[51] S. Saravanan, and N. Ramesh Babu, "RBFN based MPPT Algorithm for PV System with High Step-Up Converter," *Energy Conversion and Management*, vol. 122, pp. 239-251, 2016. *Crossref*, https://doi.org/10.1016/j.enconman.2016.05.076

[52] Ahmed Ismail M.Ali, Mahmoud A.Sayed, and TakaharuTakeshita, "Isolated Single-Phase Single-Stage DC-AC Cascaded Transformer-Based Multilevel Inverter for Stand-Alone and Grid-Tied Applications," *International Journal of Electrical Power & Energy Systems*, vol. 125, p. 106534, 2021. *Crossref*, https://doi.org/10.1016/j.ijepes.2020.106534

[53] Souradeep Pal et al., "A Cascaded Nine-Level Inverter Topology with T-Type and H-Bridge with Increased DC-Bus Utilization," *IEEE Transactions on Power Electronics*, vol. 36, no. 1, pp. 285-294, 2021. *Crossref*, https://doi.org/10.1109/TPEL.2020.3002918

[54] Zhen Shao, and Zhengrong Xiang, "Design of an Iterative Learning Control Law for a Class of Switched Repetitive Systems," *Circuits, Systems, and Signal Processing*, vol. 36, no. 2, pp. 845-866, 2016. *Crossref*, https://doi.org/10.1007/s00034-016-0331-6

[55] Akbar Ahmad, and P. Samuel, "Photovoltaic System-Based Marx Multilevel Converter for Hybrid Modulation Strategy," *Lecture Notes in Electrical Engineering*, pp. 567-574, 2017. *Crossref*, https://doi.org/10.1007/978-981-10-4286-7_56